Photochemistry and Photobiology, 2007, 83: 603–610

Energetics of Cytosine Singlet Excited-State Decay Paths—A Difficult Case for CASSCF and CASPT2†

Lluís Blancafort

Departament de Química, Institut de Química Computacional, Universitat de Girona, Campus de Montilivi, Girona, Spain

Received 29 May 2006; accepted 28 September 2006; published online 3 October 2006; DOI: 10.1562/2006-05-29-RA-903

ABSTRACT

Three deactivation paths for singlet excited cytosine are calculated at the CASPT2//CASSCF (complete active space second-order perturbation//complete active space self-consistent field) level of theory, using extended active spaces that allow for a reliable characterization of the paths and their energies. The lowest energy path, with a barrier of approximately 0.1 eV, corresponds to torsion of the C_5–C_6 bond, and the decay takes place at a conical intersection analogous to the one found for ethylene and its derivatives. There is a further path with a low energy barrier of approximately 0.2 eV associated with the (n_N,π^*) state which could also be populated with a low energy excitation. The path associated with a conical intersection between the ground and (n_O,π^*) states is significantly higher in energy (> 1 eV). The presence of minima on the potential energy surface for the (n,π^*) states that could contribute to the biexponential decay found in the gas phase was investigated, but could not be established unequivocally.

INTRODUCTION

The photophysics of DNA bases has been studied in great detail in recent years, thanks to the development of spectroscopic methods and their increase in resolution (1–4). Their general characteristic is the short lifetime of the singlet excited state, which lies in the picosecond and sub-picosecond range. In the case of cytosine, the decay in the gas phase was first described as monoexponential with a lifetime of 3.2 ps (3), while more recently a biexponential decay with components of 0.16 and 1.9 ps has been measured (5). In addition to the ultrashort components, a long living dark state (lifetime of approximately 300 ns) has been measured in the gas phase with a photoionization technique (6). The decay of cytidine in water has been measured as monoexponential, with a lifetime of 0.5–0.8 ps (1,2).

One common theoretical approach to explain the experimental features is based on the excited-state potential energy surfaces. In this approach, the ultrafast decay is associated with one or more points of conical intersection (crossings between states of the same multiplicity) between the ground and excited states (7–10). These points should be energetically accessible to account for the ultrafast lifetimes. Several paths of this type have been identified for the decay of singlet excited cytosine to the ground state (11–16). A first paper described two paths, associated with the (n_O,π^*) and (n_N,π^*) excited states (excitation coming from the oxygen and nitrogen lone pairs, respectively) (11). The (n_O,π^*) decay was associated with a bond inversion of the conjugated system and had the lower energy barrier at the CASSCF (complete active space self-consistent field) level. A following CASPT2 (complete active space with second-order perturbation) study, where dynamic correlation energy is added to the CASSCF treatment, suggested that the conical intersection found for the bond inversion path involved the (π,π^*) state (12). The role of the (n_O,π^*) and (π,π^*) states and the presence of a three-state crossing was discussed in a further CASPT2 and CASSCF study (13). More recently, independent DFT/MRCI (density functional/multireference configuration interaction) (15) and CR-EOM-CCSD(T)//CIS (completely renormalized equation of motion coupled cluster and configuration interaction with singles, respectively) (14,16) studies showed the existence of a further path with low barriers, associated with torsion of the C_5–C_6 bond (see atom numbering in Fig. 1). This path had been suggested earlier for the cytosine–guanine Watson–Crick pair on the basis of CASPT2 calculations (17). A point that supports the relevance of this path is that it accounts for the longer excited-state lifetime of 5-fluoro cytosine compared with its parent compound (18), as it involves out-of-plane bending of the C_5 substituent (fluorine or hydrogen in each case). In contrast, calculations on the bond inversion path could not explain the differences in the excited-state lifetimes between the two compounds (18).

While the comparison of the lifetime of cytosine with its 5-fluoro derivative is one way to assess the relevance of the calculated paths, another possibility is to compare the calculated energy barriers. In the case of cytosine, the pathways described above were calculated at different levels of theory, and their energetics are difficult to compare. Therefore the main purpose of the present study was to recalculate the different paths with a consistent theoretical treatment. The calculations follow the CASPT2//CASSCF approach, where the minimum energy paths on the excited state are optimized at the CASSCF level and the energies recalculated with CASPT2 (19). As explained below, special care has been applied in choosing an active space for the CASSCF calculation that avoids some of the pitfalls of this approach, so as to provide a reliable and homogeneous description of the potential energy surface and a meaningful comparison of the different paths.

†This invited paper is part of the Symposium-in-Print: DNA Photodynamics.

*Corresponding author email: lluis.blancafort@udg.es (Lluís Blancafort)

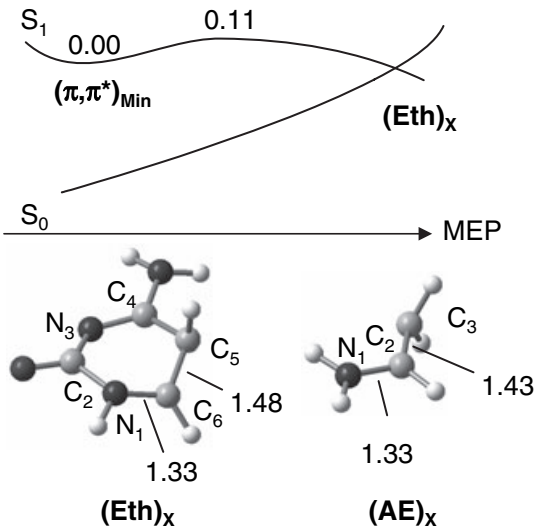

Figure 1. Energy profile for decay of singlet excited cytosine along ethylenic path (torsion of C_5–C_6 bond). $\mathbf{(AE)_X}$ is the conical intersection analog for aminoethylene.

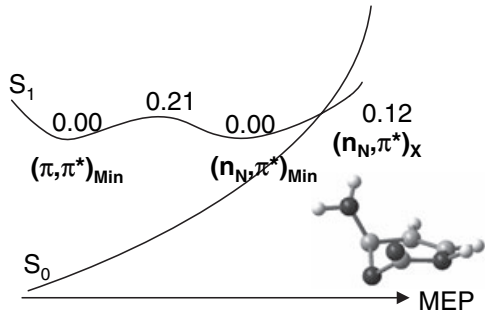

Figure 2. Energy profile for decay of singlet excited cytosine along (n_N,π^*) path (out-of-plane bending of N_1).

In summary, the results show that the energetically favored decay path involves the torsion of the C_5–C_6 bond, with an estimated barrier of 0.1 eV (Fig. 1). The conical intersection has been characterized as an analog of the one found between the ground and excited states of ethylene and its derivatives. The decay along the (n_N, π^*) path also has a small barrier of approximately 0.2 eV (Fig. 2), while the barrier along the bond inversion path is significantly higher (>1 eV). A further point of interest is the role of the (n,π^*) states in the photophysics, in view of the biexponential decay observed recently (5). In a semiclassical picture, the biexponential decay could arise from two different minima on the surface, one being the minimum of the spectroscopic (π,π^*) state, $\mathbf{(\pi,\pi^*)_{Min}}$, and the other one an (n,π^*) state minimum. An alternative would be to assign the short lifetime component to decay from the Franck-Condon region to $\mathbf{(\pi,\pi^*)_{Min}}$ (or even direct decay to the conical intersection with the ground state, surmounting the small energy barriers), and the longer component to the $\mathbf{(\pi,\pi^*)_{Min}}$ intermediate. This alternative has been investigated by identifying the minima for the (n,π^*) states and calculating the barriers that separate them from $\mathbf{(\pi,\pi^*)_{Min}}$, but no definitive conclusions could be reached concerning the contribution of the (n,π^*) minima to the photophysics.

MATERIALS AND METHODS

General computational details. The calculations were carried out at the CASSCF and CASPT2 levels of theory, using the 6-31+G* basis set. Thus, the excited-state optimizations and minimum energy path calculations were carried out at the CASSCF level using the Gaussian03 program (20), while the CASPT2 energies were recalculated with single point calculations using the Molcas5.4 program (21). In all cases, the barriers are given as the energy difference between the minimum of the spectroscopic state, $\mathbf{(\pi,\pi^*)_{Min}}$, and the point of highest energy along the reaction coordinate.

CASSCF wavefunction. The CASSCF calculations were carried out with active spaces of 9–12 orbitals, and the active space choice is explained below in detail. Structures $\mathbf{(\pi,\pi^*)_{Min}}$, $\mathbf{(n_N,\pi^*)_{Min}}$, [minima of the ($\pi$,$\pi^*$) and ($n_N$,$\pi^*$) states, respectively], $\mathbf{(n_N,\pi^*)_X}$ and $\mathbf{(n_O,\pi^*)_X}$ [conical intersections between the ground state and the (n_N,π^*) and (n_O,π^*) states, respectively], $\mathbf{(Eth)_X}$ (conical intersection of ethylenic type between ground and excited state), and $\mathbf{(Eth)_{TS}}$ [transition structure between $\mathbf{(\pi,\pi^*)_{Min}}$ and $\mathbf{(Eth)_X}$], were optimized using state average over two states (S_0 and S_1) with equal weights. For a better convergence of the wavefunction, the CASSCF optimizations on S_1 of $\mathbf{(n_O,\pi^*)_{Min}}$ [minimum of the (n_O,π^*) state] and $\mathbf{(n_N,\pi^*)_{TS}}$ [transition structure between $\mathbf{(\pi,\pi^*)_{Min}}$ and $\mathbf{(n_N,\pi^*)_{Min}}$] were carried out stateaveraging over three states (S_0, S_1 and S_2) with equal weights. The same procedure was used for the intrinsic reaction coordinate (IRC) calculations from $\mathbf{(n_N,\pi^*)_{TS}}$ to $\mathbf{(\pi,\pi^*)_{Min}}$ and $\mathbf{(n_N,\pi^*)_{Min}}$. The IRC calculations from $\mathbf{(Eth)_{TS}}$ to $\mathbf{(Eth)_X}$ and $\mathbf{(\pi,\pi^*)_{Min}}$, as well as the IRC from $\mathbf{(n_N,\pi^*)_X}$ to $\mathbf{(n_N,\pi^*)_{Min}}$ were also carried out stateaveraging over two states.

Active spaces. The active space for the (n_O,π^*) path aims to get the same ordering of the S_0, S_1 and S_2 states at the CASSCF and CASPT2 levels, and get similar S_0–S_1 and S_1–S_2 energy gaps at both levels of theory. Test calculations were carried out at the conical intersection between the ground and (n_O,π^*) states optimized at the CASSCF (8,7)/6-31G* level of theory (11). The problem at this structure is that with the "natural" (12,9) active space made of the 8 π type orbitals and the n_O orbital, the order of the S_1 and S_2 states is inverted at the CASSCF and CASPT2 levels (Table S1, Supplemental Materials) (12). Thus the active space was extended with additional orbitals, namely the σ and σ^* orbitals localized on the C–O bond, and two orbitals centered mainly on the oxygen atom. One of these is dominated by the antibonding combination of the 2p and 3p in-plane basis functions and is labeled n_O^*. The other orbital is the out-of-plane analog and is labeled p_O^*. The inclusion of the σ orbitals on the C–O bond is justified because the bond is significantly stretched along the (n_O,π^*) path, while the n_O^* orbital is included to improve the correlation for the oxygen in plane lone pair. The p_O^* orbital further improves the balance between the (π,π^*) and (n_O,π^*) states. In addition, the active π orbital localized mainly on the amino group was removed from the active space to improve the convergence and save computational time, as it has an occupation larger than 1.99. This gives a (12,12) active space (12 electrons in 12 orbitals). With this active space, the state inversion does not occur (see Table S1), but the state degeneracy between S_0 and S_1 is lost. Therefore structures $\mathbf{(n_O,\pi^*)_{Min}}$ and $\mathbf{(n_O,\pi^*)_X}$ were reoptimized with this active space. In fact, tests with different active spaces (see Table S1) show that the state inversion can be avoided with smaller active spaces, but the (12,12) active space was chosen for the optimizations as it gives the best agreement between the CASSCF, CASPT2 and MS-CASPT2 (multistate formulation of CASPT2) (19) energies [compare the S_1–S_2 gaps with (12,11) and (12,12) active spaces in Table S1].

For the (n_N,π^*) path, the CASPT2 profile along the CASSCF minimum energy path optimized with a (10,8) active space (7 π orbitals and n_N lone pair) is discontinuous (see Figs. S1 and S2, Supplemental Materials). Following the strategy described for the (n_O,π^*) path, the CASSCF optimizations are repeated with a (12,11) active space composed of 7 π orbitals, the n_N lone pair, the σ and σ^* orbitals localized on the N_3–C_4 bond, and the n_N^* orbital on the N_3 atom. With this (12,11) active space, good agreement is obtained between the CASSCF and CASPT2 energy profiles (see Figs. 3 and 4, respectively). For the first part of the (n_N,π^*) path [$\mathbf{(\pi,\pi^*)_{Min}}$ to $\mathbf{(n_N,\pi^*)_{Min}}$ along $\mathbf{(n_N,\pi^*)_{TS}}$], the wavefunction is calculated for the three lowest states, while for the second part [optimization of $\mathbf{(n_N,\pi^*)_X}$ and IRC to $\mathbf{(n_N,\pi^*)_{Min}}$, see Fig. 5] the wavefunction is calculated for the two lowest states. In this case, the CASSCF calculation converged to an active

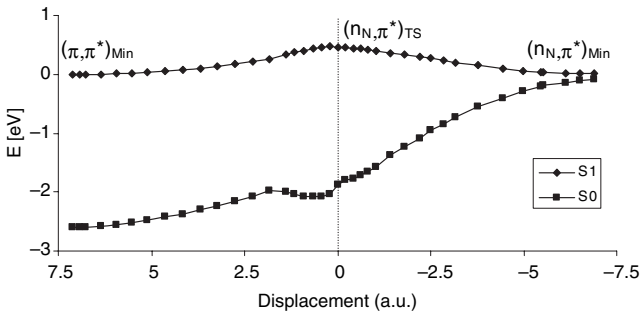

Figure 3. CASSCF optimized minimum energy path for the first part of the (n_N,π^*) path.

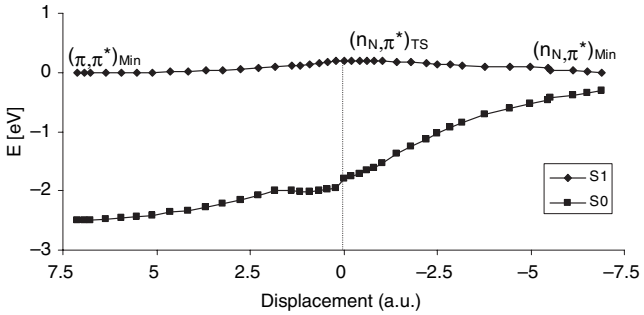

Figure 4. CASPT2 energy profile along CASSCF minimum energy path for the first part of the (n_N,π^*) path.

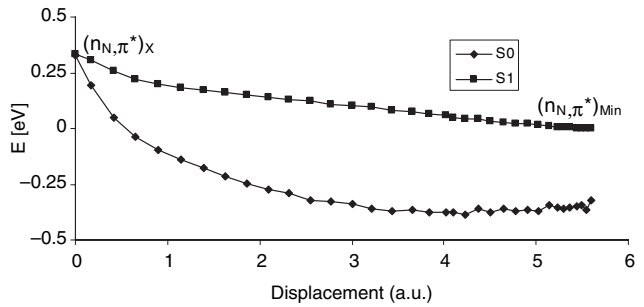

Figure 5. CASSCF optimized minimum energy path for the second part of the (n_N,π^*) path.

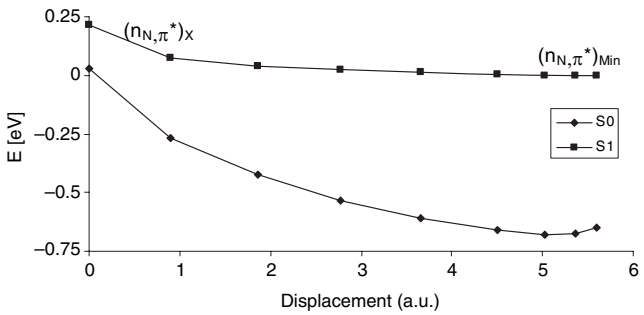

Figure 6. CASPT2 energy profile along CASSCF minimum energy path for the second part of the (n_N,π^*) path.

space where the orbital localized on the amino group replaced one of the ring π orbitals. For consistency with the first part of the path, the CASPT2 profile (Fig. 6) is calculated with a CASSCF(12,11) wavefunction averaged over three states with equal weights.

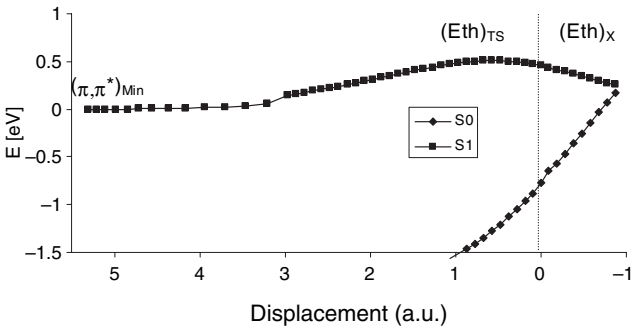

Figure 7. CASSCF optimized minimum energy path for ethylenic path.

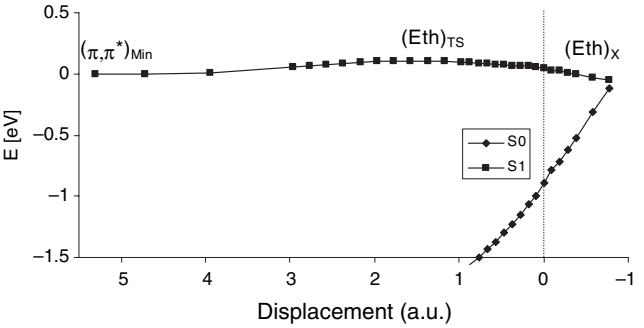

Figure 8. CASPT2 energy profile along CASSCF minimum energy path for ethylenic path.

For the ethylenic path (Figs. 7 and 8) the two σ and σ^* orbitals localized on the C_5–C_6 bond were added to the seven π orbitals of lowest occupation to give a (10,9) active space.

The strategy used for the active space selection, where the aim is to recover the most significant part of dynamic correlation for each state at the CASSCF level, precludes the use of the same active space for the different paths, as this would lead to active spaces of unpractical size and would cause convergence problems. Therefore the absolute energies for structures lying along different paths are not comparable, and the barriers along the paths reflect relative values. However, the CASPT2 correction should moderate this effect, as shown for the vertical excitations. These were calculated using the (12,12) and (12,11) active spaces described for the (n_O,π^*) and (n_N,π^*) paths, respectively (see Table 1). These calculations give the vertical excitation energies for the (π,π^*) and (n_O,π^*) pair of states, and the (π,π^*) and (n_N,π^*) pair, respectively, and the CASPT2 (π,π^*) excitations are similar. Thus the active spaces used for the two paths give consistent results, and the relative energies can be compared. Besides, to study the effect of including the π orbital on the NH_2 substituent in the active space, the

Table 1. CASSCF and CASPT2 photophysical energies of lowest singlet states calculated with different active spaces (ground-state geometry optimized at the CASSCF(8,7)/6-31 G* level).

Active space[a]	States	E_{CASSCF} [eV]	E_{CASPT2} [eV]
(12,12)	$(\pi,\pi^*)_{vert}$	5.49	4.51
	$(n_O,\pi^*)_{vert}$	6.16	5.59
	$(\pi,\pi^*)_{0\text{-}0}$	4.18	3.75
	$(\pi,\pi^*)_{em.max}$	3.09	2.98
(14,13)	$(\pi,\pi^*)_{vert}$	5.31	4.55
	$(n_O,\pi^*)_{vert}$	6.05	5.52
(12,11)	$(\pi,\pi^*)_{vert}$	5.57	4.46
	$(n_N,\pi^*)_{vert}$	6.00	5.26

[a]See full text.

(π,π^*) and (n_O,π^*) vertical excitations were recalculated with a (14,13) active space. Again, the difference between the CASPT2 excitations with a (12,12) and (14,13) active space is small.

The 6-31 + G* basis set was used to improve the convergence of the wavefunction because of the n* and p* orbitals included in the active space. Rydberg contamination of the valence states is possible but seems unlikely in the present case as the occupations of the n* and p* active orbitals, which have the largest components of diffuse basis functions, are less than 0.02. In addition, the CASPT2 (π,π^*) vertical excitation is similar to the one calculated with the 6-31G* basis, which shows that there is no artificial energy lowering caused by Rydberg mixing. Moreover, test calculations performed on the structures along the (n_O,π^*) path, supplementing the 6-31G* basis with diffuse functions only on the oxygen atom, give similar results to the ones with the 6-31 + G* basis.

CASSCF optimizations and minimum-energy paths. In the optimizations and minimum-energy path calculations [IRC calculations (22)], the orbital rotation corrections to the gradients were not calculated because they require the solution of the coupled perturbed multi-configuration self-consistent field equations (23), which is computationally not feasible for an active space of more than eight orbitals with the present Gaussian code. The use of approximate gradients caused an inaccuracy in the determination of the minimum energy path for the ethylenic decay. Thus, the IRC from $\mathbf{(Eth)_{TS}}$ in the direction of $\mathbf{(\pi,\pi^*)_{Min}}$, calculated at the CASSCF level, gives a small energy rise during the first steps of the IRC, and the highest energy point along the coordinate lies 0.05 eV higher than $\mathbf{(Eth)_{TS}}$ (see Fig. 7). Besides, frequency calculations are not possible with large active spaces at present, and therefore the optimized transition structures were characterized with frequency calculations using smaller (8,7) active spaces. The IRC calculations were started using these force constants.

Structure $\mathbf{(n_O,\pi^*)_X}$ could not be fully optimized because the intersection has a sloped topology (24) with almost parallel ground and excited-state gradients, which causes inaccuracies in the conical intersection optimization gradient. Instead, a point of degeneracy was located by using only the energy difference component of the conical intersection gradient for the optimization (25). The starting point for the partial optimization was a structure with a small energy gap found during the attempted full optimization. Further optimization of $\mathbf{(n_O,\pi^*)_X}$ would lower its energy. However, no substantially lower points with small energy gaps could be found during the attempted full optimizations, and the energy of $\mathbf{(n_O,\pi^*)_X}$ [approximately 1.3 eV relative to $\mathbf{(\pi,\pi^*)_{Min}}$] is a reasonable upper bound to the optimum value.

Valence-bond analysis of $\boldsymbol{(Eth)_X}$ *and* $\boldsymbol{(AE)_X}$ *conical intersections*. To characterize the decay path along the C_5–C_6 torsion, the S_1/S_0 conical intersection analog for aminoethylene, $\mathbf{(AE)_X}$, was optimized at the CASSCF(4,3)/6-31 G* level. To complete the analysis, $\mathbf{(Eth)_X}$ and $\mathbf{(AE)_X}$ were characterized with a valence-bond based analysis which uses the $\alpha\beta$ components of the active-space spin-exchange one electron density (26), computed with localized active orbitals. The interpretation of the spin-exchange one electron density matrix elements (P_{ij}) has been discussed previously (27). In short, values of 0.4 or higher, approximately, are a sign of localized double bond character between atoms *i* and *j*. In addition, the diagonal elements of the active-space one electron density matrix (D_{ii}), calculated with localized orbitals, give a measure of the charge distribution on the atoms and the possible charge transfer character of the states. The calculations were carried out with active spaces of 7 and 3 π orbitals for $\mathbf{(Eth)_X}$ and $\mathbf{(AE)_X}$, respectively, for a correct localization. The results are given in Tables S2–S5 (Supplemental Materials), and the resonance structures derived from this analysis are shown in Fig. 9.

CASPT2 calculations. The CASPT2 single point calculations along the IRC profiles were carried out with the CASSCF reference function used for the corresponding IRC calculation, except for the final part of the (n_N,π^*) path (see subsection Active spaces). To obtain the energy barriers along the paths, the energies of the stationary points were recalculated at the same level (including active space, number of states in the CASSCF reference state and level shift parameter) than the corresponding IRC calculation. A real level shift parameter (28) was used for all CASPT2 calculations. The value of the parameter was chosen so as to get similar reference weights (within 1%) for all states along the paths, while keeping it as small as possible. It was 0.2 for all calculations except for the ethylenic decay path, where a parameter of 0.15 was used.

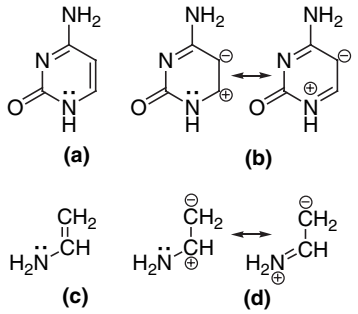

Figure 9. Resonance structures for the degenerate states at $\mathbf{(Eth)_X}$ (a, b) and $\mathbf{(AE)_X}$ (c, d).

RESULTS

Methodological considerations

The use of the CASPT2//CASSCF approach is not straightforward (19), and it has proved to be rather challenging for the present case. Thus, to produce good energy estimates the CASPT2 energy profile has to be similar to the optimized CASSCF one; otherwise, the CASPT2 profile may be discontinuous. Another problem may be inversion in the order of the states between the two methods. This problem occurs when states which are close at the CASSCF level have different correlation energy, which can cause the order of the states to change when going to CASPT2. This happened in previous CASPT2//CASSCF calculations along the bond inversion path of cytosine, and it made the assignment of the crossing states as (π,π^*) or (n_O,π^*) problematic (12,13). In order to overcome these problems, the active space for the CASSCF optimizations has been extended beyond the "natural" one formed by the π orbitals and the lone pairs involved directly in the excitations. The idea is to increase the correlation energy included in the CASSCF calculation, so as to approach the CASPT2 results. By including specifically those orbitals in the active space that are related to the relevant excited states and the geometric coordinates of each path, the agreement between the CASSCF and CASPT2 profiles has been greatly improved. However this occurs at the expense of computational time, as the number of CASSCF configurations increases greatly and convergence of the CASSCF wavefunction is slowed down because of the presence of orbitals with low occupations. In addition, the need to approximate the gradients with large active spaces can also lead to some inaccuracies, as seen for the ethylenic path. Moreover, the results for the (n_O,π^*) path are somewhat unsatisfactory, as the CASSCF and CASPT2 profiles are qualitatively quite different (see Fig. 10). A further extension of the active space would be desirable here. However the (12,12) active space is a limitation for the computational capacity available for this work, and it is also not clear which orbitals could be included to improve the calculations.

Vertical excitations

The vertical excitations of the three lowest excited states, calculated with different active spaces (see General

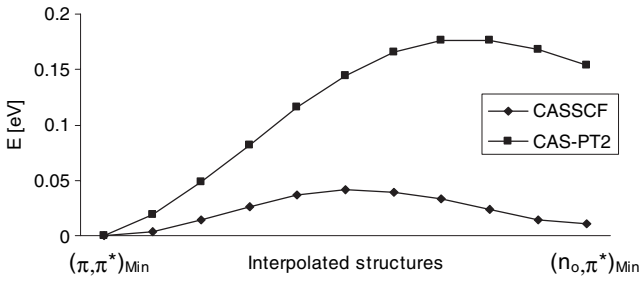

Figure 10. CASPT2 and CASSCF energy profiles along linear interpolation coordinate between $(\pi,\pi^*)_{Min}$ and $(n_O,\pi^*)_{Min}$.

computational details), are shown in Table 1. The CASSCF energy of the (π,π^*) state depends on the active space, but the CASPT2 energies agree within 0.1 eV. The estimated energy of approximately 4.5 eV for the lowest (π,π^*) state agrees well with previous CASPT2 calculations, which gave approximately the same value (12), and with the experimental gas phase absorption maximum of 4.65 eV obtained recently in electron energy loss spectroscopic measurements (29). Moreover, the calculated Stokes shift is approximately 1.5 eV. While the value is considerably higher than the experimental value of 0.81 eV, measured in water, it is smaller than the one of approximately 2.0 eV calculated previously with a smaller active space and basis set (18). The two lowest (n,π^*) states come out higher in energy, and the (n_N,π^*) state lies approximately 0.3 eV lower than the (n_O,π^*) one (5.3 and 5.6 eV, respectively). Thus the order of the (n_N,π^*) and (n_O,π^*) excitations changes with respect to previous CASPT2 calculations using a smaller active space for the CASSCF reference wavefunction, where the (n_O,π^*) state comes out lower than the (n_N,π^*) one (12). Recent DFT/MRCI calculations also give the (n_O,π^*) state as the lowest (n,π^*) state (15). While the calculated (n_N,π^*) excitation of approximately 5.3 eV (CAS(12,11)-PT2) agrees well with the previous values of 5.2 eV (CAS(12,9)-PT2) and 5.5 eV (DFT/MRCI), the difference between the previous results and the present ones lies mainly in the (n_O,π^*) energy. It was calculated as 5.0 eV at the DFT/MRCI level and 4.9 at the CAS(12,9)-PT2 level, while it is approximately 5.6 eV here, at the CAS(12,12)-PT2 level. The test calculations described in the General computational details section show that the (12,12) active space gives a better description of the (n_O,π^*) state, and therefore the value of 5.6 eV should be more reliable. However, because of the small oscillator strength, there are no experimental data to assess the accuracy of the calculations for the (n_O,π^*) states.

Ethylenic path

The minimum energy path for the radiationless decay along the ethylenic route, optimized at the CASSCF level of theory, is presented in Fig. 7, and the CASPT2 energetics along the path in Fig. 8. The path leads to the conical intersection $\mathbf{(Eth)_X}$. The barrier is 0.51 eV at the CASSCF level, and 0.11 eV at the CASPT2//CASSCF level. $\mathbf{(Eth)_X}$ is optimized at the CASSCF level. The CASPT2 energy gap at $\mathbf{(Eth)_X}$ is 0.13 eV, and 0.06 eV at the last point of the IRC from $\mathbf{(Eth)_{TS}}$ to $\mathbf{(Eth)_X}$. Structure $\mathbf{(Eth)_X}$ is characterized by a twist of the C_5–C_6 bond, and the twisting angle (H–C_5–C_6–H dihedral) is 118º. The major changes in bond lengths, with respect to the ground state minimum, are the lengthening of the C_5–C_6 bond from 1.35 to 1.48 Å, and a shortening of the N_1–C_6 bond from 1.37 to 1.33 Å, in agreement with previous calculations (14–16). The remaining bond lengths do not change by more than 0.01 Å, approximately.

The crossing states are characterized with a valence-bond based analysis in terms of the resonance structures shown in Fig. 9. Structure 9a corresponds to the ground-state resonance structure at the FC geometry, with a bonding interaction between the π electrons on C_5–C_6 (see the P_{ij} elements in Table S2, Supplemental Materials). Structure 9b is ionic (see the D_{ii} elements in Table S3, Supplemental Materials), with a net negative charge on C_5 and a positive one on C_6, stabilized by resonance with the π electron pair on N_1. There is also no π bonding between C_5 and C_6 for this state (see the P_{ij} elements in Table S2, Supplemental Materials). Thus the intersection is of the same type as the well-known intersection of ethylene (30–35) and its derivatives (36–40), where the ground state crosses a zwitterionic excited state. In fact an analogous conical intersection structure has been optimized for aminoethylene, with a twist angle of 111° for the C–C bond (H–C_3–C_2–N_1 dihedral) (Fig. 1), and similar bond lengths. The crossing states for the aminoethylene intersection have the same resonance structures than the ones of $\mathbf{(Eth)_X}$ in cytosine (Fig. 9c,d, P_{ij} and D_{ii} values shown in Tables S4 and S5, respectively, Supplemental Materials).

(n_N,π^*) Path

The minimum energy path from $\mathbf{(\pi,\pi^*)_{Min}}$ to the $\mathbf{(n_N,\pi^*)_X}$ conical intersection consists of two parts. The first part goes to an excited-state minimum, $\mathbf{(n_N,\pi^*)_{Min}}$, and the second part continues to the $\mathbf{(n_N,\pi^*)_X}$ intersection. The CASSCF optimized path between the two minima, which corresponds to a state switch between the spectroscopic (π,π^*) state and the (n_N,π^*) one, is shown in Fig. 3, and the CASPT2 energies in Fig. 4. The energy gap between the ground and excited states at $\mathbf{(n_N,\pi^*)_{Min}}$ is 0.09 eV at the CASSCF level, and 0.31 eV at the CASPT2 level. The path from $\mathbf{(n_N,\pi^*)_{Min}}$ to $\mathbf{(n_N,\pi^*)_X}$ was calculated with a different active space (see General computational details). With that active space, the energy gap at $\mathbf{(n_N,\pi^*)_{Min}}$ is larger (0.32 and 0.65 eV at the CASSCF and CASPT2 level, respectively), and the energy barrier to the intersection is 0.33 eV at the CASSCF level and 0.12 eV with CASPT2 (see the energy profiles in Figs. 5 and 6, respectively). At the CASPT2 level, the energy gap between the ground and excited states at $\mathbf{(n_N,\pi^*)_X}$ is 0.19 eV. The out-of-plane bending of N_3 at the intersection has been previously explained as coming from electron repulsion due to the (n_N,π^*) excitation (11).

(n_O,π^*) Path

The conical intersection between the (n_O,π^*) state and the ground state, $\mathbf{(n_O,\pi^*)_X}$ has a sloped topology. Full optimization was not possible (see General computational details), but the calculations give upper bounds of approximately 1.25 and 1.55 eV for the energy relative to $\mathbf{(\pi,\pi^*)_{Min}}$ at the CASSCF level and CASPT2 levels, respectively. The S_1/S_0 energy gap at the CASPT2 level is 0.29 eV. Thus the energy barriers are substantially higher than the ones calculated for the other two

paths, and it seems unlikely that full optimization of the intersection would change this significantly. In addition, a minimum for the (n_O,π^*) state, $(\mathbf{n_O},\pi^*)_{\mathbf{Min}}$, was optimized at the CASSCF level of theory on the S_1 surface. $(\mathbf{n_O},\pi^*)_{\mathbf{Min}}$ has virtually the same energy as $(\pi,\pi^*)_{\mathbf{Min}}$ at the CASSCF level (it lies 0.01 eV higher), and it lies 0.15 eV higher at the CASPT2 level. Optimization of the transition structure between the two minima has not been possible due to the flatness of the surface at the CASSCF level, but a linear interpolation (Fig. 10) gives a barrier of less than 0.1 eV and approximately 0.2 eV at the CASSCF and CASPT2 levels, respectively.

DISCUSSION

According to CASPT2//CASSCF calculations with extended active spaces, the energetically preferred decay pathway of singlet excited cytosine to the ground state is the one associated with torsion of the C_5–C_6 bond, with a calculated barrier of approximately 0.1 eV (Fig. 1). The barrier to the conical intersection along the bond inversion path [(n_O,π^*) path] is substantially higher (>1.4 eV). Besides, the barrier along the (n_N,π^*) decay path (out-of-plane bending of the N_1 atom) is approximately 0.2 eV with respect to $(\pi,\pi^*)_{\mathbf{Min}}$ (Fig. 2). The barrier lies well below the vertical excitation energy [which is approximately 0.8 eV over $(\pi,\pi^*)_{\mathbf{Min}}$, see Table 1], which suggests that this path can also contribute to the ultrafast decay. In water the energy barrier for this path will be higher, presumably, due to the blue shift of the (n_N, π^*) state.

The conical intersection for the lowest-energy path has been characterized as an analog of the conical intersection for ethylene. For ethylene it is known that the twisting of the C–C double bond does not lower the energy of the ionic state enough to reach degeneracy with the ground state (30,32). Instead, the intersection occurs at a structure where the ionic state is stabilized by partial migration of one hydrogen (31,33,35,41), and theoretical calculations suggest that part of the excited-state population decay occurs in the hydrogen migration region (42,43). In cytosine the ionic state is stabilized by the π electron pair on N_1 and the lowest-energy conical intersection has no hydrogen migration component. The same occurs for amino ethylene (Fig. 1). Thus, the fragment responsible for the excited-state decay along this path is the N_1–C_6–C_5 group of the ring, and the presence of the electron pair on N_1 prevents the hydrogen migration during the decay at the intersection. The same applies for the decay of singlet excited uracil and thymine, which go through the same mechanism (14,44).

As for the minima of the (n,π^*) states, which could account for the biexponential decay (5), two such minima could be located for the (n_O,π^*) and (n_N,π^*) states. However their role in photophysics could not be clarified completely. Thus $(\mathbf{n_O},\pi^*)_{\mathbf{Min}}$ looks like a shallow minimum at the CASPT2 level, lying 0.15 eV higher than $(\pi,\pi^*)_{\mathbf{Min}}$. Re-optimization of $(\mathbf{n_O},\pi^*)_{\mathbf{Min}}$ at a more correlated level would lower its energy. However, $(\mathbf{n_O},\pi^*)_{\mathbf{Min}}$ optimized at a more correlated level could also come out on the S_2 potential energy surface instead of S_1, in which case it would be more difficult to be accessed from $(\pi,\pi^*)_{\mathbf{Min}}$. As for $(\mathbf{n_N},\pi^*)_{\mathbf{Min}}$, the energy gap to the ground state at this structure is small (<1 eV) and the conical intersection $(\mathbf{n_N},\pi^*)_{\mathbf{X}}$ lies close to the minimum. At the same time, because of the use of approximate gradients in the calculations (see General computational details), it cannot be excluded that the minimum is a spurious critical point, and that the IRC from $(\mathbf{n_N},\pi^*)_{\mathbf{TS}}$ leads directly to $(\mathbf{n_N},\pi^*)_{\mathbf{X}}$ [the energy gap at $(\mathbf{n_N},\pi^*)_{\mathbf{Min}}$, at the CASSCF level, is <0.1 eV]. Apart from their possible contribution to the decay, previous calculations suggest that the (n,π^*) states could be important in providing access to the triplet state thanks to the spin-orbit coupling between the (n,π^*) and (π,π^*) states of different multiplicity (45). Calculations on the triplet state at the improved level of theory are currently in progress to reevaluate this possibility.

Acknowledgements—This work was supported by the Ramón y Cajal program from the Spanish Ministerio de Educación y Ciencia (MEC), grant CTQ2005-04563 from the Dirección General de Investigación (MEC), a grant from the Francesca Roviralta Foundation and a research grant from the Universitat de Girona (Ref. 7E200402).

SUPPLEMENTAL MATERIALS

The following supplemental materials are available for this article:

Figure S1. CASSCF(8,7)/6-31G* optimized minimum energy path for first part of (n_N,π^*) path.

Figure S2. CAS(12,9)-PT2 energy profile along CASSCF(8,7)/6-31G* minimum energy path for first part of (n_N,π^*) path.

Table S1. CASSCF, CASPT2 and MS-CASPT2 energies of the three lowest singlet states (relative to S_0) with different active spaces (6-31+G* basis), calculated at the conical intersection between the ground and (n_O,π^*) states optimized at the CASSCF(8,7)/6-31G* level.

Table S2. Bond orders (spin-exchange one electron density matrix elements, P_{ij}) between localized active space orbitals for cytosine $(\mathbf{Eth})_{\mathbf{X}}$ structure (atom numbering see Fig. 1).

Table S3. Occupations of localized active space orbitals (diagonal elements of one-electron density matrix, D_{ii}) for cytosine $(\mathbf{Eth})_{\mathbf{X}}$ structure (atom numbering see Fig. 1).

Table S4. Bond orders (spin-exchange one electron density matrix elements, P_{ij}) between localized active space orbitals for aminoethylene $(\mathbf{AE})_{\mathbf{X}}$ structure (atom numbering see Fig. 1).

Table S5. Occupations of localized active space orbitals (diagonal elements of one-electron density matrix, D_{ii}) for aminoethylene $(\mathbf{AE})_{\mathbf{X}}$ structure (atom numbering see Fig. 1).

This material is available as part of the online article from: http://www.blackwell-synergy.com/doi/full/10.1562/2006-05-29-RA-903

Please note: Blackwell Publishing are not responsible for the content or functionality of any supplementary materials supplied by the authors. Any queries (other than missing material) should be directed to the corresponding author for the article.

REFERENCES

1. Pecourt, J. M. L., J. Peon and B. Kohler (2001) DNA excited-state dynamics: Ultrafast internal conversion and vibrational cooling in a series of nucleosides. *J. Am. Chem. Soc.* **123**, 10370–10378.
2. Peon, J. and A. H. Zewail (2001) DNA/rna nucleotides and nucleosides: Direct measurement of excited-state lifetimes by

femtosecond fluorescence up-conversion. *Chem. Phys. Lett.* **348**, 255–262.
3. Kang, H., K. T. Lee, B. Jung, Y. J. Ko and S. K. Kim (2002) Intrinsic lifetimes of the excited state of DNA and rna bases. *J. Am. Chem. Soc.* **124**, 12958–12959.
4. Crespo-Hernández, C. E., B. Cohen, P. M. Hare and B. Kohler (2004) Ultrafast excited-state dynamics in nucleic acids. *Chem. Rev.* **104**, 1977–1202.
5. Canuel, C., M. Mons, F. Piuzzi, B. Tardivel, I. Dimicoli and M. Elhanine (2005) Excited states dynamics of DNA and rna bases: Characterization of a stepwise deactivation pathway in the gas phase. *J. Chem. Phys.* **122**, 074316.
6. Nir, E., M. Muller, L. I. Grace and M. S. de Vries (2002) Rempi spectroscopy of cytosine. *Chem. Phys. Lett.* **355**, 59–64.
7. Klessinger, M. and J. Michl (1995) *Excited States and Photochemistry of Organic Molecules*. VCH Publishers, Inc., New York.
8. Bernardi, F., M. Olivucci and M. A. Robb (1996) Potential energy surface crossings in organic photochemistry. *Chem. Soc. Rev.* **25**, 321–328.
9. Migani, A. and M. Olivucci (2004) Conical intersections and organic reaction mechanisms. In *Conical Intersections. Electronic Structure, Dynamics and Spectroscopy* (Edited by W. Domcke, D. R. Yarkony and H. Köppel), pp. 271–322. World Scientific Publishing Co. Pte. Ltd., Singapore.
10. Blancafort, L., F. Ogliaro, M. Olivucci, M. A. Robb, M. J. Bearpark and A. Sinicropi (2005) Computational investigation of photochemical reaction mechanisms. In *Computational Methods in Photochemistry* (Edited by A. G. Kutateladze), pp. 31–110. CRC Press, Boca Raton, FL.
11. Ismail, N., L. Blancafort, M. Olivucci, B. Kohler and M. A. Robb (2002) Ultrafast decay of electronically excited singlet cytosine via π,π^* to $n_{(o)}\pi^*$ state switch. *J. Am. Chem. Soc.* **124**, 6818–6819.
12. Merchán, M. and L. Serrano-Andrés (2003) Ultrafast internal conversion of excited cytosine via the lowest π,π^* electronic singlet state. *J. Am. Chem. Soc.* **125**, 8108–8109.
13. Blancafort, L. and M. A. Robb (2004) Key role of a threefold state crossing in the ultrafast decay of electronically excited cytosine. *J. Phys. Chem. A* **108**, 10609–10614.
14. Zgierski, M. Z., S. Patchkovskii, T. Fujiwara and E. C. Lim (2005) On the origin of the ultrafast internal conversion of electronically excited pyrimidine bases. *J. Phys. Chem. A* **109**, 9384–9387.
15. Tomic, K., J. Tatchen and C. M. Marian (2005) Quantum chemical investigation of the electronic spectra of the keto, enol, and keto-imine tautomers of cytosine. *J. Phys. Chem. A* **109**, 8410–8418.
16. Zgierski, M. Z., S. Patchkovskii and E. C. Lim (2005) Ab initio study of a biradical radiationless decay channel of the lowest excited electronic state of cytosine and its derivatives. *J. Chem. Phys.* **123**.
17. Sobolewski, A. L. and W. Domcke (2004) Ab initio studies on the photophysics or the gu-cy base pair. *Phys. Chem. Chem. Phys.* **6**, 2763–2771.
18. Blancafort, L., B. Cohen, P. M. Hare, B. Kohler and M. A. Robb (2005) Singlet excited-state dynamics of 5-fluorocytosine and cytosine: An experimental and computational study. *J. Phys. Chem. A* **109**, 4431–4436.
19. Serrano-Andrés, L., M. Merchán and R. Lindh (2005) Computation of conical intersections by using perturbation techniques. *J. Chem. Phys.* **122**, 104–107.
20. Frisch, M. J., G. W. Trucks, H. B. Schlegel, G. E. Scuseria, M. A. Robb, J. R. Cheeseman, J. J. A. Montgomery, T. Vreven, K. N. Kudin, J. C. Burant, J. M. Millam, S. S. Iyengar, J. Tomasi, V. Barone, B. Mennucci, M. Cossi, G. Scalmani, N. Rega, G. A. Petersson, H. Nakatsuji, M. Hada, M. Ehara, K. Toyota, R. Fukuda, J. Hasegawa, M. Ishida, T. Nakajima, Y. Honda, O. Kitao, H. Nakai, M. Klene, X. Li, J. E. Knox, H. P. Hratchian, J. B. Cross, C. Adamo, J. Jaramillo, R. Gomperts, R. E. Stratmann, O. Yazyev, A. J. Austin, R. Cammi, C. Pomelli, J. W. Ochterski, P. Y. Ayala, K. Morokuma, G. A. Voth, P. Salvador, J. J. Dannenberg, V. G. Zakrzewski, S. Dapprich, A. D. Daniels, M. C. Strain, O. Farkas, D. K. Malick, A. D. Rabuck, K. Raghavachari, J. B. Foresman, J. V. Ortiz, Q. Cui, A. G. Baboul, S. Clifford, J. Cioslowski, B. B. Stefanov, G. Liu, A. Liashenko, P. Piskorz, I. Komaromi, R. L. Martin, D. J. Fox, T. Keith, M. A. Al-Laham, C. Y. Peng, A. Nanayakkara, M. Challacombe, P. M. W. Gill, B. Johnson, W. Chen, M. W. Wong, C. González and J. A. Pople (2003) *Gaussian03 Revision b.02*. Gaussian, Inc., Pittsburgh, PA.
21. Andersson, K., M. Barysz, A. Bernhardsson, M. R. A. Blomberg, Y. Carissan, D. L. Cooper, M. Cossi, T. Fleig, M. P. Fülscher, L. Gagliardi, C. d. Graaf, B. A. Hess, G. Karlström, R. Lindh, P.-Å. Malmqvist, P. Neogrády, J. Olsen, B. O. Roos, B. Schimmelpfennig, M. Schütz, L. Seijo, L. Serrano-Andrés, P. E. M. Siegbahn, J. Stålring, T. Thorsteinsson, V. Veryazov, M. Wierzbowska and P. O. Widmark (2003) *Molcas Version 5.4*. University of Lund, Sweden.
22. González, C. and H. B. Schlegel (1990) Reaction-path following in mass-weighted internal coordinates. *J. Phys. Chem.* **94**, 5523–5527.
23. Yamamoto, N., T. Vreven, M. A. Robb, M. J. Frisch and H. B. Schlegel (1996) A direct derivative mc-scf procedure. *Chem. Phys. Lett.* **250**, 373–378.
24. Atchity, G. J., S. S. Xantheas and K. Ruedenberg (1991) Potential-energy surfaces near intersections. *J. Chem. Phys.* **95**, 1862–1876.
25. Bearpark, M. J., M. A. Robb and H. B. Schlegel (1994) A direct method for the location of the lowest energy point on a potential surface crossing. *Chem. Phys. Lett.* **223**, 269–274.
26. Deumal, M., J. J. Novoa, M. J. Bearpark, P. Celani, M. Olivucci and M. A. Robb (1998) On the validity of the mcconnell-i model of ferromagnetic interactions: The [2.2]paracyclophane example. *J. Phys. Chem. A* **102**, 8404–8412.
27. Blancafort, L., P. Celani, M. J. Bearpark and M. A. Robb (2003) A valence-bond-based complete-active-space self-consistent-field method for the evaluation of bonding in organic molecules. *Theor. Chem. Acc.* **110**, 92–99.
28. Roos, B. O. and K. Andersson (1995) Multiconfigurational perturbation-theory with level shift—The cr-2 potential revisited. *Chem. Phys. Lett.* **245**, 215–223.
29. Abouaf, R., J. Pommier, H. Dunet, P. Quan, P. C. Nam and M. T. Nguyen (2004) The triplet state of cytosine and its derivatives: Electron impact and quantum chemical study. *J. Chem. Phys.* **121**, 11668–11674.
30. Buenker, R. J., V. Bonačić-Koutecký and L. Pogliani (1980) Potential-energy and dipole-moment surfaces for simultaneous torsion and pyramidalization of ethylene in its lowest-lying singlet excited-states—A cl study of the sudden polarization effect. *J. Chem. Phys.* **73**, 1836–1849.
31. Ohmine, I. (1985) Mechanisms of nonadiabatic transitions in photoisomerization processes of conjugated molecules—Role of hydrogen migrations. *J. Chem. Phys.* **83**, 2348–2362.
32. Bonačić-Koutecký, V., J. Koutecký and J. Michl (1987) Neutral and charged biradicals, zwitterions, funnels in s1, and proton translocation—Their role in photochemistry, photophysics, and vision. *Angew. Chem. Int. Ed. Engl.* **26**, 170–189.
33. Freund, L. and M. Klessinger (1998) Photochemical reaction pathways of ethylene. *Int. J. Quantum Chem.* **70**, 1023–1028.
34. Ben-Nun, M. and T. J. Martínez (2000) Photodynamics of ethylene: Ab initio studies of conical intersections. *Chem. Phys.* **259**, 237–248.
35. Barbatti, M., J. Paier and H. Lischka (2004) Photochemistry of ethylene: A multireference configuration interaction investigation of the excited-state energy surfaces. *J. Chem. Phys.* **121**, 11614–11624.
36. Bonačić-Koutecký, V., K. Schoffel and J. Michl (1987) Critically heterosymmetric biradicaloid geometries of protonated schiff-bases—Possible consequences for photochemistry and photobiology. *Theor. Chim. Acta* **72**, 459–474.
37. Barbatti, M., A. J. A. Aquino and H. Lischka (2005) A multireference configuration interaction investigation of the excited-state energy surfaces of fluoroethylene (c2 h3f). *J. Phys. Chem. A* **109**, 5168–5175.
38. Pitonak, M. and H. Lischka (2005) Excited-state potential energy surfaces of silaethylene: A mrci investigation. *Mol. Phys.* **103**, 855–862.
39. Barbatti, M., A. J. A. Aquino and H. Lischka (2006) Ultrafast two-step process in the non-adiabatic relaxation of the ch2nh2+ molecule. *Mol. Phys.* **104**, 1053–1060.
40. Zechmann, G., M. Barbatti, H. Lischka, J. Pittner and V. Bonacic-Koutecky (2006) Multiple pathways in the photodynamics of a

polar pi-bond: A case study of silaethylene. *Chem. Phys. Lett.* **418**, 377–382.
41. Ben-Nun, M. and T. J. Martínez (1998) Ab initio molecular dynamics study of cis-trans photoisomerization in ethylene. *Chem. Phys. Lett.* **298**, 57–65.
42. Barbatti, M., M. Ruckenbauer and H. Lischka (2005) The photodynamics of ethylene: A surface-hopping study on structural aspects. *J. Chem. Phys.* **122**.
43. Barbatti, M., G. Granucci, M. Persico and H. Lischka (2005) Semiempirical molecular dynamics investigation of the excited state lifetime of ethylene. *Chem. Phys. Lett.* **401**, 276–281.
44. Matsika, S. (2004) Radiationless decay of excited states of uracil through conical intersections. *J. Phys. Chem. A* **108**, 7584–7590.
45. Merchán, M., L. Serrano-Andrés, M. A. Robb and L. Blancafort (2005) Triplet-state formation along the ultrafast decay of excited singlet cytosine. *J. Am. Chem. Soc.* **127**, 1820–1825.